Commissioning Measurements On An Elekta Unity MR-Linac

Marcus Powers (marcus.powers@my.jcu.edu.au)
James Cook University https://orcid.org/0000-0002-4235-6123
John Baines
Townsville Hospital and Health Service
Robert Crane
Townsville Hospital and Health Service
Chantelle Fisher
Townsville Hospital and Health Service
Stephen Gibson
Townsville Hospital and Health Service
Linda Marsh
Townsville Hospital and Health Service
Bronwyn Shirley
Townsville Hospital and Health Service
Ariadne Shoobridge
Townsville Hospital and Health Service
Marchant Van der Walt
Townsville Hospital and Health Service
Glenn de Vine
Townsville Hospital and Health Service

Research Article

Keywords: MR-Linac, Commissioning, Elekta Unity

Posted Date: September 21st, 2021

DOI: https://doi.org/10.21203/rs.3.rs-873957/v1

Version of Record: A version of this preprint was published at Physical and Engineering Sciences in Medicine on March 2nd, 2022. See the published version at https://doi.org/10.1007/s13246-022-01113-7.

Abstract

MR-guided radiotherapy technology is relatively new and commissioning publications, QA protocols and commercial products are limited. This work provides guidance for implementation measurements that may be performed on the Elekta Unity MR-Linac (Elekta, Stockholm, Sweden). Adaptions of vendor supplied phantoms facilitated determination of gantry angle accuracy and MV isocentre, whereas in-house developed phantoms were used for End-to-End (E2E) testing and anterior coil attenuation measurements. Third-party devices were used for measuring beam quality, reference dosimetry and during IMRT commissioning; however, due to several challenges, variations on standard techniques were required. Gantry angle accuracy was within 0.1°, confirmed with pixel intensity profiles, and MV isocentre diameter was < 0.5 mm. Anterior coil attenuation was < 0.6 %. Beam quality as determined by $TPR_{20,10}$ was 0.704 ± 0.002, in agreement with treatment planning system (TPS) calculations, and gamma comparison against the TPS for a 22.0 × 22.0 cm^2 field was above 95.0 % (2.0 %, 2.0 mm). G90 output was 1.000 ± 0.002 Gy per 100 MU, depth 5.0 cm. During IMRT commissioning, sub-standard results indicated issues with machine behaviour. Once rectified, gamma comparisons were above 95.0 % (2.0 %, 2.0 mm). Centres which may not have access to specialized equipment can use in-house developed phantoms, or adapt those supplied by the vendor, to perform commissioning work and confirm operation of the MRL within published tolerances. The IMRT QA devices and techniques used in this work highlight issues with machine behaviour when appropriate gamma criteria are set.

Introduction

The integration of MR imaging and MV beam generation achieved with the Elekta Unity MRL (Elekta, Stockholm, Sweden) design presents quality assurance challenges. Following the on-site construction of the system, Elekta personnel perform device acceptance tests (DAT) that replace conventional linac acceptance tests. Commissioning and beam modelling validation measurements are also performed by Elekta personnel, with Philips staff responsible for MR image quality testing. Prior to clinical go-live, a period of quality assurance follows during which in-house physicists perform baseline quality assurance and validation measurements across both MR and MV modalities. Elekta tests incorporate specialised QA devices and analysis software that are not necessarily commercially available. Furthermore, due to the presence of the magnetic field, conventional equipment available to the clinic may not be compatible with the Unity system.

The design of the Unity system has been comprehensively discussed by other investigators, [1–5] and the reader is referred to these works for further information. In short, the Elekta Unity MRL is a combination of a modified Philips Ingenia 1.5 T MRI with a split-coil superconducting magnet and a straight-through linear accelerator. The beam generation system, producing a single 7 MV FFF x-ray source, is mounted on an annular gantry that is free to rotate around a cylindrical cryostat containing the static-field MR coils. The axis of gantry rotation and the central axis of the coils are coincident, with the static magnetic field (B_0) in the negative Y direction (IEC61217) as shown in Fig. 1. For all gantry angles the beam passes

through the cryostat and is perpendicular to B_0. The angular dependent beam transmission through the cryostat (aluminium annular structure containing liquid helium) is referred to as the cryostat characterisation and will vary between Unity systems mostly due to differences in construction of the cryostat annulus; however, a small component will be due to differences in helium fill [3]. A modified Elekta Agility® Beam Limiting Device (BLD) shapes fields ranging from 0.8 × 0.5 cm^2 to 57.4 × 22.0 cm^2 at isocentre, with a fixed dose-rate at this point of 425.0 MU/min. The patient positioning system (PPS) is capable of longitudinal movement only and the isocentre is 14.0 cm above the PPS, 143.5 cm from the source. A fixed EPID panel, now called the mega-voltage imager (MVI) [5], diametrically opposite the x-ray source on the gantry is capable of MV portal imaging a maximum field size of 22.0 × 9.5 cm^2, for QA purposes only. A schematic of the MR-linac is shown in Fig. 1, courtesy of Elekta.

The Elekta Unity MRL in conjunction with the Monaco v5.40 treatment planning system, enables real-time adaptive radiotherapy planning. Within Monaco, the GPU Monte Carlo dose (GPUMCD) algorithm is used for fast, Monte Carlo dose calculations in the presence of a static 1.5 T magnetic field [6, 7]. Dose calculations are performed on voxelized models of patient or QA phantom datasets with relative electron density (RED) assigned per voxel based on a CT specific, user defined CT number to RED table. For calculations performed on MR datasets, RED information is assigned on a per structure basis with user specified values; typically, the mean RED for a structure is calculated from a reference CT scan. REDs are converted to mass densities, with the result mapped to chemical composition using Patient, Phantom or Couch material look-up tables. Users can specify a dose calculation grid resolution and statistical uncertainty to control the accuracy and duration of calculations. For plan adaptation two workflows are available, Adapt-to-Position (ATP) or Adapt-to-Shape (ATS). ATP involves repositioning of pre-treatment (reference) plan isocentre based on the rigid registration of that plan and image dataset with a daily MR image. The pre-treatment plan can be recalculated or reoptimized on the reference dataset to reproduce or improve target dose coverage. ATS allows for plan adaption based on anatomical changes as shown on the daily MR image. Contours can be automatically deformed to match the daily anatomy, with optional user-based adjustments. The reference plan is recalculated or reoptimized using reference plan constraints [8]. For more information on the replanning options the reader is referred to other works [6–8].

Published work focused on commissioning of the Elekta Unity system is limited [3–5, 9]. Recently, the work of Roberts et al [3] provides tolerances and frequencies for common QA tests and Woodings et al [5] for acceptance procedures on the linac component. Since this technology has only recently been clinically introduced (results reported in this work were obtained with the first Unity in the Southern Hemisphere), there is currently no region-specific guidance for implementation and safe use of the MRL, as is the current situation for conventional treatment systems [10]; however, position papers are unlikely to vary significantly from the recommendations of the above investigators [3, 5]. It is the intention that our work will aid clinics introducing an Elekta Unity and provide benchmarks for test results not previously reported.

Although numerous commissioning tests may be performed on an Elekta Unity, only a subset are presented below. Adaptions of the Elekta supplied MV alignment phantom (Fig. 2(a)) enabled

independent verification of the gantry angle accuracy and reproducibility and the MV isocentre, whereas development of in-house phantoms was required for measurements of beam attenuation due to the anterior imaging coil and End-to-End (E2E) testing. Difficulties were encountered when measuring beam quality and output, and when performing IMRT commissioning, with commercial equipment that required adaptions to standard methodologies and as such are also presented below. During installation there was limited time to facilitate customer selected measurements prior to magnet ramp up. A spontaneous quench and planned ramp down events enabled selected commissioning tests to be repeated with B = 0 T. More common commissioning measurements, for example mechanical behaviour of the system, MR-to-MV isocentre offset confirmation, relative dosimetry measurements, a thorough investigation of the treatment planning system (TPS) and the commissioning of the MR system are not provided in this work for conciseness. That work, together with MLC characterisation, mutual interference of MR and MV systems and a radiation survey within the treatment room will be published separately.

Due to the construction of the gantry ring, the use of an inclinometer to determine gantry angle is limited to 270.0° [5]. As part of routine QA for conventional linacs it is common to determine gantry angle accuracy for multiple positions and to assess the reproducibility of gantry rotation. A unique phantom design has been proposed for such measurements on the Elekta Unity MRL [11]; however, in the absence of such a phantom we propose the use of a vendor supplied equipment, Fig. 2(a) and Fig. 2(b), that can be adapted to investigate gantry angle positioning.

During device acceptance tests (DAT) an Elekta supplied Cryostat Characterisation Tool (CCT), see Fig. 2(c) is used with the MVI to obtain a series of images of a ballbearing for MV isocentre determination. These images are forwarded to Elekta for analysis using Radiation Isocentre Tool (RIT) software v6.6.64 (Radiological Imaging Technologies, Colorado Springs, Colorado, USA). Alternatively, Snyder et al [4] described the use of the MV alignment phantom, Fig. 2(a), to obtain MVI images of the centrally located ballbearing; however, image analysis relied on access to RIT software. In this work we demonstrate the use of the same phantom and central ballbearing to determine the MV-isocentre with in-house software analysis, and a comparison of this this methodology with those mentioned above is provided.

For all treatments on the Unity the anterior imaging coil is present above the patient and should be fully characterised in terms of it is dosimetric impact on treatment beams [5, 9]. The use of an in-house phantom to determine coil attenuation for a selection of gantry angles is described. Furthermore, a default coil model is provided in the Monaco TPS and a comparison of calculated and measured attenuation is presented.

The beam quality specifier for the Elekta Unity MRL is the $TPR_{20,10}$ [9, 12-14], consistent with the recommendations of the TRS-398 protocol, and due to its insensitivity to the magnetic field [9, 13, 14]. Due to the difficulties with measuring PDDs, a direct measurement of $TPR_{20,10}$ is preferred and with the presence of the cryostat, slight angular dependence of beam quality could be expected. With the quality dependent factors for reference output, such as $k_{B_{\parallel},Q}$ [13, 14] and k_{Q,Q_0}, a determination of this

angular dependence, or at minimum an assessment of the change in these factors with beam quality, should be evaluated.

During DAT on the recommendation of Elekta the MRL was calibrated to give 1.000 Gy per 100 MU to isocentre, at 5.0 cm depth in water, for a 10.0 × 10.0 cm^2 field, G90. Measuring from G90 is the preferred methodology due to the constancy of the helium fill at this angle compared to acute anterior angles, like G0, where the output may vary depending on the level of helium. However, other users report a calibration depth of 10.0 cm to maximize the delivered dose-rate [4] thereby reducing treatment times.

The PTW 1D water tank (PTW, Freiburg, Germany) is often used for output determination with the dosimetry protocol proposed by van Asselen et al [13]. When using the current version of the PTW 1D tank, a direct measurement of the output at isocentre for a chamber depth of 5.0 cm in water cannot be achieved at G90. Future versions of the PTW tank will address this issue; however, at present an adaption of the formalism in van Asselen et al [13] is required for clinics calibrating the Unity consistent with the Elekta advice. Calibration in a plastic water phantom was avoided due to variation in response of the chamber due to the presence of air gaps generating and the electron return effect (ERE) [14, 15].

As part of the Elekta beam validation procedure, nine vendor IMRT plans, based on AAPM TG-199 [16] guidance, were imported to the Monaco treatment planning system (TPS) and delivered on the Unity system. Elekta recommends gamma criteria of 3.0 % (global dose), 3.0 mm DTA during beam validation with the ArcCheck®-MR device (Sun Nuclear, Melbourne, Fl, USA). This device was not available during commissioning and in its absence the Octavius 1500^{MR} (PTW, Freiburg, Germany) and Gafchromic™ EBT3/EBT-XD film (Ashland ISP Advanced Materials, NJ, USA) were utilized. The methodology for planning system calculations and the various measurement techniques are provided below.

Elekta provides phantoms for ATP and ATS E2E testing on the Unity during Physics Validation; however, a clinic may want to perform their own measurements for routine QA and, for example, during treatment site commissioning. Purchasing specific phantoms for individual site development can be expensive and furthermore, a centre may not have ready access to commercial phantoms for adaptive radiotherapy E2E testing. The use of in-house developed 3D printed phantoms can alleviate these issues. 3D printed materials have been extensively used in conventional radiotherapy applications [17–19] and their use in MR-guided radiotherapy (MRgRT) systems has seen much development [20, 21]. An in-house designed phantom with 3D printed components was used for E2E measurements for baseline comparisons on the Unity in this work.

Clearly, Unity users encounter challenges performing independent routine determination of common QA tests, such as those listed above. Due to the complexity of the Unity and the variety of possible tests, it is likely that physicists will not find comparative values in current publications for all commissioning work performed locally. The significance of our work is in the novel measurement techniques that describe alternative uses for vendor supplied phantoms and the use of in-house developed phantoms. Additionally, this work provides useful baseline results for future Unity users.

Methods

Gantry Angle

The vendor supplied phantom shown in Fig. 2(a) facilitates determination of the MV isocentre size and position. In this work, the phantom has been adapted to assess the accuracy of gantry angle positioning. This cylindrical, Perspex phantom contains a centrally located, 10.0 mm diameter ballbearing and at each outer edge of the cylinder there are twelve 4.0 mm ballbearings radially arranged at 30.0° angular intervals. The centre of each ballbearing array is offset by 3.5 cm from the central ballbearing. With this phantom positioned on the Elekta supplied QA platform (see Fig. 2(b)) MVI images of the phantom were obtained at the cardinal gantry angles using 20.0 × 9.5 cm^2 fields, 20 MU, and analysed using vendor supplied software to determine the offset of the phantom from the radiation isocentre (translations and rotations). The phantom was then repositioned using the QA platform with X, Y and Z vernier adjustments. Additional MVI images were used to confirm the phantom position until the offsets were less than 0.2 mm and 0.2° in all directions. The phantom was then shifted ± 3.5 cm in the Y-direction so that the centre of a given array of ballbearings was nominally at the isocentre.

MVI images of the phantom were obtained with the gantry angle varying from 0.0° to 360.0° in 30.0° increments using a 10.0 × 10.0 cm^2 field, 50 MU. At each angle diametrically opposite ball bearings should eclipse and nominally an image of a single ballbearing would be produced. Furthermore, the separation between ballbearings at the image peripheries should vary from the nominal G0 image depending on the gantry angle. Visual inspection of the images was performed to confirm this. MVI images were also obtained with the gantry rotated ± 1.0° from vertical in increments of ± 0.1° to assess the resolution of the relevant ballbearings (twelve o'clock and six o'clock). The gantry angle was measured with a digital Clinotronic PLUS inclinometer (Wyler AG, Winterthur, Switzerland) between each rotation to confirm the relative shift from G0. A self-levelling laser was used to confirm that the ballbearings at twelve and six o'clock were aligned vertically within the phantom. In addition to visual inspection of the images, pixel value profiles were extracted using ImageJ v1.53a (NIH, Bethesda, MD, USA) [22]. Profiles across each MVI image through the centre of all ballbearings were obtained for all selected gantry angle and compared to that for the G0 image.

MV Isocentre Diameter

For our determination of the MV Isocentre size, the MV alignment phantom (Fig. 2(a)) was mounted on the QA Platform and aligned to the isocentre using the methodology described above. With the centre of the phantom at the isocentre, the central ballbearing was projected onto the MVI using 5.0 × 5.7 cm^2, 50 MU, fields every 10.0° for gantry angles ranging from 0.0° – 360.0°. In contrast to the methodology used by Snyder et al [4] and Elekta, gantry angles of 10.0° and 20.0° were avoided, due to the presence of the cryostat cross-over pipe that provides electrical connection between the split coils, and angles of 60.0° and 300.0° due to interference from the couch edges through the centre of the ballbearing image. Images with the gantry moving both clockwise (CW) and counter-clockwise (CCW) were obtained in a single

sequence, for a total of sixty-nine projections. The images were exported from the MVI computer and analysed with in-house MATLAB® code (MathWorks, Natick, Massachusetts, USA). Vertical and horizontal pixel intensity profiles were extracted from each MVI images to determine the ballbearing position.

When imaging from 130.0° to 50.0° and 310.0° to 230.0°, the phantom, QA platform and couch edges created distortion in the images. To minimize this effect, horizontal background pixel profiles just above and below the ballbearing were acquired for a given projection, averaged, and then subtracted from the horizontal profile through the ballbearing. The process was repeated for vertical profiles just to the right and left of the ballbearing. The FWHM of the ballbearing is then more accurately determined from the resulting profiles. The centre pixel of the FWHM peak is then compared against the MVI central pixel for each projection to determine the MV isocentre. Note that the coincidence of the MVI central pixel to the radiation field isocentre was confirmed during commissioning at multiple gantry angles, the method for which is outside the scope of this work. The routine use of this technique requires accurate and consistent beam steering, and this should be ensured by clinics before adopting this method; however, is not expected to vary significantly over time [5].

To validate the use of the MV alignment phantom and beam sequence for determining the MV isocentre size as described above, the CCT was irradiated using the same developed sequence and method. Also, the MV alignment phantom was irradiated using the fields required for RIT, consistent with the method of Snyder et al [4] and Elekta. Isocentre sizes were compared between phantoms, beam sequences and magnetic field environments. During the in-house Physics validation measurements, spoke shot films were obtained with GafchromicTM RTQA2 (Ashland ISP Advanced Materials, NJ, USA) film following the methodology proposed by [3, 23] wherein copper rings are introduced. The spoke shot dose distribution under the rings is less influenced by the interaction of electrons with the magnetic field, improving the precision of the isocentre determination in the X-Z plane. These results are also provided for comparison.

Anterior Coil Attenuation

The attenuation of the anterior imaging coil as function of gantry angle was determined with a PTW 30013 Farmer chamber within an in-house cylindrical water-filled phantom of diameter 6.0 cm and length 15.0 cm. The long axis of the chamber was coincident with the central axis of the cylinder, see Fig. 2(d), with the Farmer threaded section and tapped cylindrical hole providing a waterproof seal. The cylindrical section of the phantom is free to rotate on two height-adjustable stands and a scale at one end facilitates rotation from 0.0° to 360.0° in 15.0° increments. The phantom was positioned in the bore with the chamber reference point positioned at the isocentre. To realise this 10.0 × 10.0 cm^2, 50 MU, A-P and L-R MVI images were used to determine necessary lateral and height adjustments. Chamber readings were obtained using a 5.0 × 5.0 cm^2 field, 100 MU, for 15.0° gantry angle increments from 75.0° to 285.0°. The cylindrical phantom was also rotated with the gantry so that the same orientation of the chamber with respect to the beam was maintained. This process was repeated with the anterior imaging coil placed in the path of the beam and corresponding readings with and without the coil were compared to determine

attenuation at each angle. The experimental arrangement was simulated in Monaco, with the water equivalent thickness of the Perspex taken into consideration when contouring. For measurements and TPS calculations, the coil height was set such that the bottom of the coil was 26.0 cm above the couch. A 0.1 cm dose grid, statistical uncertainty of 0.25 % per control point and the Patient lookup table were used for dose calculations.

X-ray Beam Quality

For $TPR_{20,10}$ measurements a PTW 30013 Farmer chamber was inserted in the PTW 1D water tank. The chamber was aligned parallel to the Y-axis with the reference point at the isocentre in the X-Y plane using A-P and L-R MVI images. Due to the size of the water tank, the chamber was lowered 4.0 cm below isocentre (- Z-direction, SCD 147.5 cm) to facilitate measurements at a depth of 20.0 cm in water. Measurements at 10.0 cm (SSD = 137.5 cm) and 20.0 cm depths (SSD = 127.5 cm) were obtained using a 10.0 × 10.0 cm^2 (at the depth of the chamber), 100 MU field at G0. $TPR_{20,10}$ was derived from the ratio of the average readings (n = 3) for each depth. To observe the effect of the variation in cryostat thickness on beam quality, $TPR_{20,10}$ measurements were also performed from G90 using a 10.0 × 10.0 cm^2 100 MU field, with the chamber at isocentre.

For profile measurements, the QA Platform was placed on the Unity couch with the patient foam mattress removed. Using four in-house 3D-printed holders, 6.5 cm depth of solid water (RW3, PTW, Freiburg, Germany) was positioned centrally on the QA Platform. With the 1500^{MR} array on top of the solid water, see Fig. 2(b), the effective point of measurement of the array was 14.0 cm above the couch. The orientation of the array with respect to the origin of the X and Y axes was checked using a 22.0 × 22.0 cm^2 MVI image of the array (G0) with an in-house aluminium “ruler” aligned on the X-axis of the array. The ruler is 2.5 cm wide and 30.0 cm in length, with thirteen machined 3.0 mm holes spaced 2.0 cm apart along its length. Misalignment of the ruler/array with the centre of the MVI image was determined using the MVI measurement tool, and array rotation was assessed against the digital grid on the image. Necessary position adjustments were identified, and the array position was adjusted using the X and Y verniers on the QA platform until the central chamber of the array was at isocentre and rotations were negligible. With the array correctly aligned the ruler was removed and 4.2 cm of solid water was positioned on the array (0.8 cm intrinsic build up) so that the detector plane was at the calibration depth of 5.0 cm. To calibrate the array a 10.0 × 10.0 cm^2 field, 100 MU, was delivered from G0 with the nominal output at 5.0 cm being 1.005 Gy for this beam (see below), as measured with a PTW 30013 Farmer-type ionisation chamber traceable to ARPANSA. Through this method the array calibration can be traced to the Australian primary standard. Finally, a 22.0 × 22.0 cm^2 gantry 0.0° field with 100 MU was delivered to the array to determine dose profiles at 5.0 cm depth

The two measurement geometries described above were simulated in the Monaco v5.40 TPS. For the $TPR_{20,10}$ simulations, two separate datasets were created for the two measurement depths. The heights of the external contours were set in Monaco such that the beam SSDs from G0 in the TPS matched the measurement geometries (137.5 cm and 127.5 cm). The width/length of the contours were set as 20.0

cm to decrease calculation time whilst maintaining full scatter conditions. For profile calculations, a 30.0 × 30.0 × 19.0 cm^3 region was contoured and set as the external structure. All three external structures were assigned a relative electron density (RED) of 1.000. TPS calculations for all geometries were performed with a 0.2 cm dose grid, 0.1 % statistical uncertainty per control point, the phantom look-up table and dose deposition to the local medium. With these settings, the statistical uncertainty at the regions of interest was less than 0.15 %. For profiles, extracted from 5.0 cm depth in the TPS, gamma analysis between calculated and measured dose maps was performed with 2.0 % local dose, 2.0 mm DTA, with dose suppression below 10.0 %, as per routine clinical practice.

Reference Dosimetry

Using the PTW 1D tank, chamber readings were acquired at isocentre for a 10.0 × 10.0 cm^2, 100 MU, field delivered from G0 to the chamber at 5.0 cm (138.5 cm SSD) and 10.0 cm (133.5 cm SSD) depths. For the same field size and MU, readings at 10.0 cm depth, G90, were acquired and corrected to 5.0 cm using the $TPR_{10,5}$ derived from G0 measurements, to give the machine output following the formalism given by van Asselen et al [13]. Chamber influence quantities for temperature and pressure, polarity and recombination, and a published magnetic field correction factor, $k_{B_{\|},Q}$ of 0.992 [13] were applied to the readings at 10.0 cm depth, G90. A non-uniformity correction factor [24] for the FFF beam was not applied given the relative flatness of the profiles at 10.0 cm depth over the dimensions of the chamber sensitive region [14]. Routinely, measuring the output from G90 using the methodology described above can be cumbersome. It is known from the cryostat attenuation that the output at isocentre for G0 is 0.5 % higher than with G90 for a 10.0 × 10.0 cm^2 field. Hence for routine QC, and as an independent check on the methodology adopted above, the output of the machine from G0 was determined relative to 1.005 Gy per 100 MU where a direct measurement at isocentre beneath 5.0 cm of water can be readily achieved. Additionally, with a ramp down event in 2021, $k_{B_{\|},M,Q}$ factors for two PTW 30013 chambers (S/N 10765 and 11298) were determined following the formalism by van Asselen et al [13]. Measurements were performed with a 10.0 × 10.0 cm^2 field, G0, at depths 5.0 cm and 10.0 cm to investigate the depth dependence of this factor.

IMRT Commissioning

Planning System Calculation

A 30.0 × 30.0 × 19.0 cm^3 solid water stack was scanned on a Toshiba Aquilion CT using 1.0 mm slices. The CT data set was imported into the QA clinic in Monaco and contoured as an external patient structure. The relative electron density of the structure was forced to 1.000 and the MRL couch structures were added, excluding the 1.0 cm foam mattress. All plans were calculated on this QA dataset described.

Following clinical practice, TPS calculations for Elekta plans used a statistical uncertainty of 3.0 % per control point and a 0.3 cm dose grid. For stereo IMRT plans, a 0.2 cm dose grid and 3.0 % statistical uncertainty per control point were used. For both settings, the overall calculated dose uncertainty was 1.0

% or lower. The phantom look-up table, with dose deposition to the local medium, was selected. For all plans, calculation times were less than 2.0 minutes.

Simple Segment Shape Check

To confirm correct MLC shaping, the segments of each stereo plan were delivered to the MVI panel. Due to the restricted imaging area of the panel (22.0 × 9.5 cm^2), this was not performed with the Elekta plans. The size, shape and position of the individual segments were visually compared to corresponding Monaco segments. Segments were delivered to the panel with gantry angles set as planned in Monaco.

Perpendicular Delivery

At our centre, film is considered the gold-standard for IMRT patient specific quality assurance (PSQA) of treatment plans on conventional linacs, with other detectors like the Octavius 1500^{MR} array being compared to film during commissioning. To this end the nine vendor IMRT plans and two in-house developed stereo plans were delivered at G0 to both film (Gafchromic EBT3 or EBT-XD, Ashland ISP Advanced Materials, NJ, USA) and an Octavius 1500^{MR} array to benchmark the array. Figure 2(b) shows the setup of the Octavius 1500^{MR} array on the QA platform for IMRT plan verification measurements. Array setup and calibration was performed with the same methodology as described above. Fields for the eleven IMRT plans were delivered perpendicularly to the array, beam-by-beam, and resulting dose maps were recorded. Comparisons of beam-by-beam dose maps and a composite dose map were made to those from the TPS. Gamma analysis was performed with Verisoft v7.2 software (PTW, Freiburg, Germany) and criteria of 2.0 % of local dose, 2.0 mm DTA and dose suppression below 10.0 %.

Depending on delivered dose per fraction, Gafchromic EBT3 film (doses less than approximately 8.0 Gy) or EBT-XD (doses greater than approximately 8.0 Gy) were also used for planar delivered dose verification with the TPS. The suitability of these film types at these dose levels has been investigated previously [25]. For film dosimetry the QA Platform was placed on the couch with the foam mattress removed and 30.0 × 30.0 × 8.0 cm^3 of solid water was placed on top with 3D printed supports (Fig. 2(b)) that nominally centre the solid water at isocentre in the X-Y plane. With this setup, the upper surface of the solid water was at isocentre height. Crosslines marked through the centre of the solid water were used to position the aluminium ruler, described above, to aid with aligning the phantom and QA platform to isocentre using the methodology described previously. After phantom alignment, film calibration was performed using a geometric dose progression with five 4.0 × 2.0 cm^2 strips of film, to encompass the maximum delivered dose for all plans [26]. The calibration was performed using 10.0 × 10.0 cm^2 G0 fields, film at 5.0 cm depth. For QA of the plans, films were centred on the solid water stack at 5.0 cm depth, and the drawn cross lines indicating the machine isocentre were marked on the film. Fields for all plans were delivered compositely from G0 to individual films. Films were scanned using an Epson 10000XL scanner at 72.0 dpi and scanner corrections were applied for the Lateral Response Artefact [27]. Comparisons to the planning system were made using FilmQA™ Pro software (Ashland ISP Advanced Materials, NJ, USA) and triple channel analysis [26]. Comparison of TPS and measured dose distributions was performed using gamma analysis with 2.0 % of global dose, 2.0 mm DTA and dose suppression below 10.0 %.

True Composite Delivery

Delivering plans perpendicularly from G0 obviously does not simulate the treatment geometry. Consequently all plans were delivered at planned gantry angles to a coronal film within a solid water block. Depending on dose level, EBT3 or EBT-XD films were used. Prior to measurement, optimal plan dependent depth for the film was identified using Monaco. Choice of depth primarily depended on beam geometry, beam weighting and the resulting dose distribution; however, typically a coronal slice was chosen through the centre of beam convergence and steep dose gradients were avoided. Film dosimetry was performed using a solid water phantom 30.0 × 30.0 × 19.0 cm^3, placed on the couch (mattress removed) and aligned to the X and Y axes using the aluminium bar and MVI images as outlined above. Fields for a given plan were delivered with the gantry angles as planned and the composite dose was captured on film at a plan specific depth of solid water. The anterior coil was excluded during measurements, and the posterior coil was included to replicate the TPS calculations. Film calibration and analysis were performed as discussed above. To investigate the potential effect of the electron return effect (ERE) on the film dose, due to the presence of air gaps between the film and solid water, measurements were repeated with the calibration and plan delivery films sprayed with water [28].

End-to-End

End-to-End (E2E) testing on the Unity was performed using an in-house designed phantom, with components 3D printed by researchers at the Royal Brisbane and Women's Hospital, Australia. The phantom comprised of a hollow Perspex cylinder (20.0 cm length, 22.0 cm diameter) containing a 3D printed frame and a platform on which 3D printed tumour surrogates could be mounted, Fig. 2(e). Surrogates were hollow, hemi-spherical and half-cylindrical shells with known internal radii and shell thickness. The hemispheres/half-cylinders could be secured together with film in-between to facilitate dosimetric measurements and were printed with holes for filling the hollow sections with MR-visible material. The platform had multiple points in which the surrogates could be inserted at known offsets for determination of fusion accuracy, MLC shaping and plan deliverability for either ATP or ATS workflows. The controlled volumes of the 3D printed surrogates can also be useful for an evaluation of the accuracy of contour auto-deformation in the ATS workflow.

The E2E water-filled phantom containing a 2.5 cm radius spherical 3D surrogate was scanned on a Toshiba Aquilion CT with 2.0 mm slices and the image dataset was imported into Monaco. Contours of the phantom and its components were defined and forced electron densities (ED) were applied to the respective mean EDs as calculated by Monaco. The water filled sections of the hemispheres were contoured together, designated as the target and set to enable automatic deformable registration. A margin expansion of 1.5 mm was applied to the target contour to generate a contour for the outer surface of the spherical shell. Dose within the phantom was calculated using a seven beam, thirty-seven segment, Step-and-Shoot IMRT (SSIMRT) plan. A 0.3 cm dose grid and 3.0 % statistical uncertainty per control point and patient look up table was used for TPS calculations. With these parameters, the statistical uncertainty was less than 0.8 % at the film location and the optimization time was 140.9 s.

To compare planned and delivered dose, the phantom was positioned on the Unity couch at the TPS couch index position. 3D printed frames attached to an accessory fixation lock bar were used to locate the phantom. The spherical surrogate was inserted in the platform offset from the centre (0.5 cm X and 1.0 cm Y), with a piece of Gafchromic EBT3 film set between the hemispheres. A 2.0 min T2-weighted image was acquired and registered to the CT dataset. An Adapt-to-Position (ATP) plan was calculated using segment shape optimization (SSO) and segment weight optimization (SWO), with the aim of reproducing goal dose [8]. Objective function parameters were not altered from their default values and the resulting recalculation time for the ATP plan was 47.8 seconds. The newly generated plan was delivered to the phantom. The spherical surrogate was replaced with a cylindrical one (with the same offsets as above) with internal radius 2.5 cm, length of 5.0 cm and a film strip positioned along its longitudinal axis. Again, a 2.0 min T2-weighted scan was acquired and registered to the CT dataset; however, now the ATS workflow was used. The auto-deformed target contour was visually checked for accuracy and manually adjusted as necessary, following clinical workflow. The ATS plan was generated from fluence with five iterations, as per the clinical default. With these settings, and the same calculation settings as for the reference plan, optimization time for the ATS plan was 149.9 seconds. Each film was compared to the planning system using FilmQA™ pro and gamma analysis with 2.0 % global dose, 2.0 mm DTA and dose suppression below 10.0 %.

Results

Gantry Angle

Representative MVI images for visual analysis of the gantry angle accuracy, reproducibility and with introduced angular offsets are shown in Fig. 3. Images have been auto enhanced within MVI to highlight pixel value gradients. With a set gantry angle of 270.0°, Fig. 3(a), the inclinometer measured an angle of 270.02°. The attenuation effect of the phantom Perspex is apparent in the 270.0° image (Fig. 3(a)) and the set angular shifts from 0.0° in Fig. 3 were confirmed to be within 0.02° with the digital inclinometer. Diametrically opposite ballbearings for all set gantry angles were eclipsed. Images every 30.0° from gantry zero were indiscernible from the G0 image, except for G270 and G90 where the thicker Perspex component of the phantom was being imaged (see Fig. 2(a)). Pixel intensity profiles for three angles are shown in Fig. 4 (G0, G0.1 and G359.9).

MV Isocentre Diameter

Results for the various isocentre measurement techniques are presented in Table 1. All techniques showed that the isocentre was within the tolerance (≤ 0.50 mm [3]).

Table 1
MV isocentre results for the various techniques configurations of phantom, analysis method, magnetic field environment

Method/Tool	Magnetic Field	Isocentre Diameter [mm]
CCT + RIT analysis	1.5 T	0.45
MV alignment + RIT analysis	1.5 T	0.42
CCT + In-house analysis	1.5 T	0.34
MV alignment + In-house analysis	1.5 T	0.38
MV alignment + In-house analysis	0 T	0.32
Spoke shot w/ Cu	1.5 T	0.36
Spoke shot w/ Cu	0 T	0.24
Spoke shot w/o Cu	0 T	0.28

Anterior Coil Attenuation

For the range of angles investigated, measured and calculated attenuation values as a function of gantry angle are shown in Table 2. The attenuation effect of the anterior coil was small, with the largest measured difference observed at G330 (0.7 %) and the largest calculated difference at G30 (1.0 %). The averaged measured attenuation was 0.5 %, with the calculated average determined to be 0.7 %.

Table 2
Differences between readings for the anterior coil present versus removal of the coil from the measurement setup. Negative values indicate the value with the anterior coil is lower

Gantry Angle [°]	Measured Attenuation [%]	Monaco Attenuation [%]
75.0	0.0	0.0
60.0	0.6	0.8
45.0	0.6	0.9
30.0	0.5	1.0
0.0	0.5	0.7
345.0	0.4	0.8
330.0	0.7	0.9
315.0	0.6	0.8
300.0	0.6	0.7
285.0	0.0	0.0

X-ray Beam Quality

The measured $TPR_{20,10}$ in the B = 1.5 T environment was 0.705 ± 0.001 (n = 4) and for the same magnetron with B = 0 T, the $TPR_{20,10}$ was 0.703 (n = 1). Planning system $TPR_{20,10}$ was calculated as 0.702 and following a magnetron replacement, the $TPR_{20,10}$ was measured as 0.703 ± 0.001 (n = 5). With the same magnetron the $TPR_{20,10}$ from G90 was 0.703 (n = 1). A dose map comparison of the measured beam with the original $TPR_{20,10}$ to the TPS is shown in Fig. 5(a) (95.3 % gamma pass rate) and similarly for the new magnetron/$TPR_{20,10}$ in Fig. 5(b) (99.6 % gamma pass rate).

Reference Dosimetry

At G0, measured output at isocentre was 1.002 ± 0.004 Gy per 100 MU (n = 7) at depth 5.0 cm, and $TPR_{10,5}$ was 0.858 ± 0.001 (n = 5). At G90, output was 1.000 ± 0.002 Gy per 100 MU (n = 7) at the isocentre under 5.0 cm of water, and similarly in the B = 0 T environment, the output at G0 was measured as 1.020 Gy per 100 MU (n = 2). At 5.0 cm depth the detector magnetic field correction factors, $k_{B_{\parallel},M,Q}$ were 0.995 (S/N 10765) and 0.996 (S/N 11298) for n = 1. With the chamber at 10.0 cm depth, $k_{B_{\parallel},M,Q}$ factors were 0.999 for both chambers. After applying the dose conversion factor $c_{\tilde{B}}$ the values for the combined magnetic field correction factors $k_{B_{\parallel},Q}$ were 0.990 (S/N 10765) and 0.991 (S/N 11298) at 5.0 cm and 0.994 for both chambers at 10.0 cm.

IMRT Commissioning

A representative segment from one of the in-house stereo plans delivered to the MVI panel is shown in Fig. 6. Comparison of this MVI image (and similar) to the TPS segment, Fig. 6(c), revealed a discrepancy between delivered MLC shapes and those calculated in the planning system, which ultimately was caused by erroneous guard leaf behaviour. Results from IMRT commissioning are shown in Tables 6–8 for both pre- and post- guard leaf fix. Values in the tables are for dry film; however, when the patient and calibration films were sprayed with water, no statistically significant variation in the gamma results were noted. This was confirmed for multiple deliveries (n = 11) across several film batches. Note that the plan names in the tables below may not necessarily match those at other Unity clinics.

Table 3

Gamma results for perpendicular deliveries to the 1500^{MR} array of the Elekta supplied TG119 plans and the two in-house developed stereo plans

Plan	Pre-Fix		Post-Fix	
	2 %, 2 mm	3 %, 3 mm	2 %, 2 mm	3 %, 3 mm
Abdomen	99.2	100.0	97.9	100.0
Head and Neck	94.2	100.0	95.8	100.0
Lung	96.4	100.0	96.1	100.0
Multi-Target	77.8	96.2	95.6	99.8
Prostate	97.4	100.0	97.8	100.0
Prostate_2	84.8	93.1	99.6	100.0
Prostate_7fld	88.4	94.8	100.0	100.0
Prostate_9fld	90.9	98.2	99.5	100.0
Prostate_11fld	96.5	100.0	100.0	100.0
Stereo 1	94.0	98.5	100.0	100.0
Stereo 2	71.2	82.0	98.6	100.0

Table 4
Gamma results for perpendicular deliveries to film of the Elekta supplied TG119 plans and the two in-house developed stereo plans

Plan	Pre-Fix		Post-Fix	
	2 %, 2 mm	3 %, 3 mm	2 %, 2 mm	3 %, 3 mm
Abdomen	96.2	99.8	96.0	99.7
Head and Neck	91.7	95.7	99.7	100.0
Lung	68.8	86.0	99.9	100.0
Multi-Target	77.4	92.9	98.0	99.9
Prostate	97.0	99.9	99.2	100.0
Prostate_2	75.7	90.5	97.6	99.7
Prostate_7fld	92.7	96.1	95.7	99.8
Prostate_9fld	95.2	99.3	97.0	100.0
Prostate_11fld	98.9	100.0	98.2	99.8
Stereo 1	70.2	92.1	97.3	99.3
Stereo 2			95.2	95.2

Table 5
Gamma results for composite deliveries to film of the Elekta supplied TG119 plans and the two in-house developed stereo plans

Plan	Pre-Fix		Post-Fix	
	2 %, 2 mm	3 %, 3 mm	2 %, 2 mm	3 %, 3 mm
Abdomen	74.5	94.7	96.5	99.7
Head and Neck	92.3	99.1	97.4	99.8
Lung	80.4	97.4	98.0	100.0
Multi-Target	79.1	94.8	97.3	99.8
Prostate	97.9	99.9	95.5	99.5
Prostate_2	87.4	97.1	96.9	99.9
Prostate_7fld			95.1	99.3
Prostate_9fld	98.0	100.0	98.8	100.0
Prostate_11fld			99.5	100.0
Stereo 1	81.2	96.3	97.8	99.6
Stereo 2			96.0	98.7

End-to-End

The ATP created plan, for an adaption of the reference CT to a daily MR with the tumour surrogate shifted, passed with an average of 99.3 % across the film RGB colour channels (2.0 % global dose, 2 mm DTA gamma criteria, dose suppression below 10.0 %). The ATS created plan, with an adaption of the reference CT to a daily MR of a cylindrical surrogate, passed with an average of 97.5 % across the three RGB colour channels.

Discussion

The results for the gantry angle measurement, as well as the MVI images in Fig. 3, highlight the accuracy of the gantry angle positioning of the Unity system. Imaging the MV alignment phantom from G270 introduced image distortions, hence G0 was chosen to determine the resolution for gantry angle reproducibility with this method. The ballbearing positions on the G0 image appear to coincide with those on the G270 image. The MVI images show that gantry angle offsets of $\geq 0.3°$ (Fig. 3(d)) from the nominal angle can be easily resolved, particularly when observing the ballbearings at image peripheries. With offsets $\leq 0.2°$ (Fig. 3(c)) images are not discernible from the nominal (no angular offset) image without further analysis of pixel intensity profiles. Obviously, visual inspection cannot be used to determine the absolute gantry angle; however, it is useful for determining if set positions are within the tolerance specified by Roberts et al [3] (± 0.3°). Note that the more recent publication of Woodings et al [5]

suggests a specification of < 0.2° for gantry angle, which cannot be achieved with this methodology unless further analysis is performed on the pixel intensity profiles, discussed below. For all projections at the 30.0° intervals, the actual gantry angle appeared to match the set position within 0.3°, further highlighting the accuracy of the gantry rotation system.

From Fig. 4 symmetry in the G0 profiles, particularly for the regions between ballbearings at image peripheries, was apparent. This symmetry, and equality between trough values, was also seen for profiles taken from the images at the 30.0° gantry angle intervals excluding G90 and G270 where image distortion interfered with the analysis. In comparison, the profiles for G0.1 (Fig. 4(a)) and G359.9 (Fig. 4(b)) show asymmetry at the peripheries, which highlights the deliberate angular offset in image acquisition. These results indicate a proof-of-concept for the use of this phantom, supplied to all Unity sites, for gantry angle QA. The process potentially could be improved by imaging with the 3.5 cm longitudinal offset removed and confirming alignment of diametrically opposed ballbearings along the Y-axis on MVI images. An absolute gantry angle offset may also be able to be determined from the offset of ballbearing centres from the lateral pixel centre on the panel; however, correct rotational alignment of the MVI would need to be confirmed, such as that discussed in [5].

The results presented in Table 1 highlight the benefit of the Unity's gantry slip-ring over conventional C-arm systems for reducing the isocentre size [4]. The isocentre diameter as measured using the CCT with the commercially available RIT software was 0.45 mm. This is larger than other reported values [4] however still within vendor tolerance (0.50 mm). The isocentre as measured with the MV alignment phantom and recommended methodology was similar in magnitude. Using our in-house method with the CCT and the MV alignment phantom, isocentre diameters were 0.34 mm and 0.38 mm, respectively, again slightly larger than that reported by Snyder et al [4]. In the 1.5 T environment, the spoke shot with copper technique, as suggested by Roberts et al [3], resulted in an isocentre comparable in magnitude to other methods. The magnetic field had a limited effect on the isocentre measurements, the largest difference observed in the spoke shots between 1.5 T and 0 T (approximately 0.1 mm).

Anterior coil attenuation for various gantry angles is shown in Table 2. Attenuation was measured as approximately 0.5 % from G0 and ranged between 0.7 % to 0.4 % for measured gantry angles. For the TPS, the G0 attenuation was 0.7 % and ranged between 0.7 % to 1.0 % across the gantry angles. Measured and calculated attenuation were consistent to within 0.5 %, with the largest discrepancy occurring at G30. Whilst the attenuation of the beam due to the anterior coil is small, the effect this has on out-of-field doses is not [29]. Baines et al [29] showed that when the anterior coil is irradiated whilst tilted, electrons ejected from the coil can spiral along magnetic field lines to deposit their doses on patient surfaces superiorly and inferiorly. In that work, doses of nearly 10.0 % of the max dose to water for a relatively small field size of 5.0 × 3.0 cm^2 were measured outside the primary field due to ESE from the coil. During patient treatments on the Unity system, where multiple gantry angles would be used, the effect of the anterior coil attenuation on the delivered dose would be negligible; however, the potential ESE should be investigated, and appropriate patient shielding should be provided.

X-ray beam quality measurements showed that at commissioning, the beam energy according to the $TPR_{20,10}$ matched the TPS within 0.5 %. The measured value was slightly higher than those reported by Snyder et al (0.704) [4], Woodings et al (0.701) [9] and van Asselen et al (0.701 ± 0.002) [13]; however, was within 0.6 % and did not significantly affect beam quality dependent chamber factors, as discussed below. The gamma comparison between measured and TPS calculated profiles agreed with the $TPR_{20,10}$ comparison, as indicated in Fig. 5(a). With the introduction of a new magnetron, the $TPR_{20,10}$ decreased approximately 0.4 % and better agreement was achieved with the TPS, Fig. 5(b), and other reported values [4, 9, 13]. Note for consistency with the TRS398 protocol [12], a 10.0 × 10.0 cm^2 field at an SCD of 147.5 cm required set field of 9.7 × 9.7 cm^2 at isocentre; however when a 10.0 × 10.0 cm^2 field at isocentre was set, the change in measured $TPR_{20,10}$ was negligible. $TPR_{20,10}$ was insensitive to the change in magnetic field strength, consistent with the work of previous investigators [9, 13, 14]. For the same magnetron the $TPR_{20,10}$ from G0 and G90 were equal within 1σ.

Other investigators calibrate the Elekta Unity MRL to deliver 1.000 Gy per 100 MU for a 10.0 × 10.0 cm^2 field from G90 to an isocentre depth of 10.0 cm in water. Linac calibration in this work was performed with the isocentre at 5.0 cm depth in water which was based on advice from Elekta to extend the life of the magnetron. Due to physical constraints the water tank does not facilitate a direct measurement at 5.0 cm depth, G90, at the isocentre. This arises as the lateral shift for the tank, required to accommodate such a chamber position, is incompatible with the size of the bore.. Reference dosimetry as performed from G90 using the $TPR_{10,5}$ adjustment was found to be reproducible, with a coefficient of variation (COV) of 0.3 %, and accurate against the nominal value of 1.000 Gy per 100 MU. The use of the $TPR_{10,5}$ reading from G0 to correct G90 readings assumes comparable beam quality between the two angles which may not be the case due to variations in cryostat construction, among other things. However, it is known from profile measurements that beam flatness at cardinal gantry angles (not shown) does not change significantly. Furthermore, the $TPR_{20,10}$ measurements from G0 and G90 were comparable and as such the change in $TPR_{10,5}$ is expected to be negligible between the two angles. Output measurements from G0 showed larger differences from the nominal value of 1.005 Gy per 100 MU and were more varied (COV = 0.5 %) as compared to G90.

Due to the difference in calibration depth in this work, the depth dependence of the detector magnetic field correction factor, $k_{B_{\parallel},M,Q}$, was investigated. Measured correction factors for the two identical Farmer type chambers at depths 5.0 cm and 10.0 cm, were consistent (within 1σ) of values reported by other investigators for the same chamber type (0.997 ± 0.002) [13]. After applying the dose conversion factor $c_{\check{B}}$ of 0.995 [13] the combined correction factors ($k_{B_{\parallel},Q}$) is consistent with the work of O'Brien et al (0.994 ± 0.001) [14] and van Asselen et al (0.992 ± 0.002) [13]. The dose conversion factor is constant at depths ranging from 5.0 cm to 25.0 cm [14], and independent of the SSD difference between published work and that for the calibration depth in this work (confirmed with Monaco simulations and beyond the scope of this work). Although the $k_{B_{\parallel},Q}$ correction factors for the two depths differ by 0.5 % they agree with published values at 10.0 cm within the measurement uncertainty of van Asselen et al [13]. This

suggests the magnetic field correction factor $k_{B_{\parallel},Q}$ is independent of depth and validates the use of published values for use at either calibration depth. This is not surprising given the previous work of O'Brien et al [30], where the dose-response of ionization chambers in a magnetic field environment tended to be depth dependent for small fields only. Strictly speaking for Unity users calibrating machines in a similar manner to this work, correction factors should be determined and applied to chamber readings taken at 10.0 cm due to the measurement setup requirements. The consistency of $TPR_{20,10}$ between G0 and G90 lends credence to measuring these factors from G0. This is in agreement with previous Monte Carlo simulations [31] which suggested that a larger $TPR_{20,10}$ change of 0.679 (6 MV linac) to 0.703 (7 MV MRL) did not influence $k_{B_{\parallel},M,Q}$ for the PTW 30013 Farmer by more than 0.5 %.

Machine output from G90 measured using the method described above was suitable for determining reference dosimetry, and measurements from G0 were adequate for routine checks. However, ideally the reference dosimetry measurement should be performed at 5.0 cm depth in water from G90 directly at the isocentre. To achieve this, equipment to be used for reference dosimetry, specifically 1D water tanks, should be designed in such a way to accommodate isocentric measurements at depths of both 10.0 cm and 5.0 cm. It is worth noting that the current magnetron on the Unity system used in this work is approaching 16.0 months of use (typical magnetron life-span when calibrating at 10.0 cm is between 9.0–12.0 months); however, this is dependent on machine load.

Initial commissioning of the Elekta supplied TG119 IMRT plans failed the departmental criteria of 2.0 %, 2.0 mm (Tables 6–9) with average pass rates of 91.7 ± 7.0 %, 88.2 ± 11.1 % and 87.1 ± 9.4 % for the Octavius perpendicular (composite comparison), film perpendicular and film composite measurements, respectively. Of note were the poor results for the Multi-Target plan and the second prostate plan across all devices. At 3.0 %, 3.0 mm gamma (as recommended during Physics Validation) results were initially considered acceptable with the average rates above 95.0 % for all three methods. Similar gamma results with criteria of 3.0 %, 2.0 mm, as per AAPM TG-218 [32], were observed. The in-house stereo plans also failed the departmental tolerance of 2.0 %, 2.0 mm and even highlighted beam delivery issues at 3.0 %, 3.0 mm. The in-house stereo plans were delivered to the MVI and visually compared segment-by-segment to the planning system, Fig. 6. It was here that the issue with the guard leaf definition in the MOSAIQ sequencer was discovered wherein the sequencer was applying an additional guard leaf rule to what was already set by the TPS. Once rectified, all plans passed above 95.0 % at 2.0 %, 2.0 mm gamma criteria, (average passes of 98.3 ± 1.8 %, 97.6 ± 1.6 % and 97.2 ± 1.3 % for the Octavius perpendicular, film perpendicular and film composite deliveries respectively). For array beam-by-beam analysis, the beams for all plans had pass rates greater than 94.5 % at 2.0 % (local dose), 2.0 mm gamma criteria. These results show that the PSQC techniques above can be used to determine issues with plan delivery. Stereo-type plans were clearly more sensitive to the guard leaf error due to the small segment sizes in the plans. As such it would be beneficial for new sites to perform their own commissioning of such plans as well as the Elekta required TG119 plans. Finally, separate comparisons between film dosimetry with and without water to the TPS revealed no statistically significant differences in gamma results between the two when using the methodology described above.

End-to-end results for both ATP and ATS created plans had pass rates > 97.0 % at 2.0 % local dose and 2.0 mm DTA. Due to the resolution of the 3D printer, the tumour surrogates housing the film were not able to be constructed airtight. This may have been of benefit as it meant that water was able to surround the film, thereby reducing uncertainties due to airgaps generating increased ERE dose. Although not a comprehensive set, the results above indicate that the use of in-house developed/3D printed phantoms can be of benefit on the Elekta Unity MRL for End-to-End purposes.

Conclusion

The MV alignment phantom can be used for gantry angle confirmation at angles other than 270.0° and visual confirmation of the set angle can be achieved within tolerance using MVI images of the phantom. The attenuation due to the anterior imaging coil is negligible and measured values agree with TPS calculations. For centres that may not have access to specialized or commercial equipment, other methods and the use of in-house phantoms have been proposed for facility-based determination of specific tests. When designing 1D water tanks, the requirements of different clinics should be considered, specifically linac calibration depths. EBT3 and EBT-XD film and the Octavius 1500^{MR} array can be used to highlight issues with plan deliverability when appropriate gamma criteria are set. Commissioning of small field plans should be considered by clinics to help highlight differences between measurements and TPS calculations.

Declarations

Acknowledgements:

We gratefully acknowledge the contribution of Emily Simpson-Page of the Royal Brisbane and Women's Hospital

Ethical Statement:

Funding

No funding was received to assist with the preparation of this manuscript.

Conflicts of interests/Competing interests

The authors have no relevant financial or non-financial interests to disclose.

Ethics approval

This article does not contain any studies with human participants or animals performed by any of the authors.

Consent

This article does not contain any patient information requiring consent.

Data Availability

All data relevant to this article can be made available upon request.

References

1. Raaymakers B, Raaijmakers A, Kotte A, Jette D, Lagendijk J (2004) Integrating a MRI scanner with a 6 MV radiotherapy accelerator: dose deposition in a transverse magnetic field. Phys Med Biol 49:4109–4118
2. Raaymakers B et al (2017) First patients treated with a 1.5 T MRI-linac: clinical proof of concept of a high precision, high-field MRI guided radiotherapy treatment. Phys Med Biol 62:41–50
3. Roberts D et al (2021) Machine QA for the Elekta Unity system: A Report from the Elekta MR-linac consortium. Med Phys 48(5):e67–e85
4. Snyder J, St-Aubin J, Yaddanapudi S, Boczkowski A, Dunkerley D, Graves S, Hyer D (2020) Commissioning of a 1.5 T Elekta Unity MR-Linac: A single institution experience. J Appl Clin Med Phys 21:160–172
5. Woodings S, de Vries J, Kok J et al (2021) Acceptance procedure for the linear accelerator component of the 1.5 T MRI-linac. J Appl Clin Med Phys 22(8):45–59
6. Hissoiny S, Ozell B, Bouchard H, Depres P (2011) GPUMCD: A new CPU-oriented Monte Carlo dose calculation platform. Med Phys 38:754–764
7. Ahmad S, Sarfehnia A, Paudel M, Kim A, Hissoiny S, Sahgal A, Keller B (2016) Evaluation of a commercial MRI Linac based Monte Carlo dose calculation algorithm with GEANT4. Med Phys 43:894–907
8. Winkel D, Bol G, Kroon P, Asselen B et al (2019) Adaptive radiotherapy: The Elekta Unity MR-linac concept. Clinical Translational Radiation Oncology 18:54–59
9. Woodings S, Bluemink J, de Vries J et al (2018) Beam characterisation of the 1.5 T MRI-linac Phys. Med Biol 63:085015
10. ACPSEM (1997) ACPSEM position paper. Recommendations for the safe use of external beams and sealed brachytherapy sources in radiation oncology. Australasian College of Physical Scientists and Engineers in Medicine. Australas Phys Eng Sci Med 20(3 Suppl.):1–35
11. Hanson I, Sullivan J, Nill S, Oelfke U (2018) OC-0079: A new multi-purpose QA phantom for use on the Elekta MR-linac. Radiother Oncol 127:S38–S39
12. Andreo P, Burns D, Hohlfeld K, Huq M, Kanai T, Laitano F, Smyth V, Vynckier S (2006) Absorbed dose determination in external beam radiotherapy: An international code of practice for dosimetry based on standards of absorbed dose to water, Technical Report TRS-398. International Atomic Energy Agency, Vienna

13. van Asselen B, Woodings S, Hackett S, van Soest T, Kok J, Raaymakers B, Wolthaus J (2018) A formalism for reference dosimetry in photon beams in the presence of a magnetic field. Phys Med Biol 63:125008
14. O'Brien D, Roberts D, Ibbott G, Sawakuchi G (2016) Reference dosimetry in magnetic fields: formalism and ionization chamber correction factors. Med Phys 43(8):4915–4927
15. Hackett S, van Asselen, Wolthaus J, Kok J, Woodings S, Lagendijk J, Raaymakers B (2016) Consequences of air around an ionization chamber: Are existing solid phantoms suitable for reference dosimetry on an MR-linac? Med Phys 43(7):3961–3968
16. Ezzell G, Burmeister J, Dogan N et al (2009) IMRT commissioning: Multiple institution planning and dosimetry comparisons, a report from AAPM Task Group 119. Med Phys 36:5359–5373
17. Van der Walt M, Crabtree T, Albantow C (2019) PLA as a suitable 3D printing thermoplastic for use in external beam radiotherapy. Australas Phys Eng Sci Med 42:1165–1176. https://doi.org/10.1007/s13246-019-00818-6
18. Dancewicz O, Sylvander S, Markwell T, Crowe S, Trapp J (2017) Radiological properties of 3D printed materials in kilovoltage and megavoltage photon beams. Physica Med 38:111–118. http://dx.doi.org/10.1016/j.ejmp.2017.05.051
19. Kairn T, Crowe S, Markwell T (2015) Use of 3D printed materials as tissue-equivalent phantoms. IFMBE Proceedings 51:728–731. https://doi.org/10.1007/978-3-319-19387-8_179
20. Niebuhr N, Johnen W, Güldaglar T et al (2016) Technical Note: Radiological properties of tissue surrogates used in multimodality deformable pelvic phantom for MR-guided radiotherapy. Med Phys 43(2):908–916. https://doi.org/10.1118/1.4939874
21. Rai R, Wang Y, Manton D, Dong B, Deshpande S, Liney G (2019) Development of multi-purpose 3D printed phantoms for MRI. Phys Med Biol 64:075010
22. Schneider C, Rasband W, Eliceiri K (2012) NIH Image to ImageJ: 25 years of image analysis. Nat Methods 9(7):671–675. https://doi.org/10.1038/nmeth.2089
23. van Zijp H, van Asselen B, Wolthaus J, Kok J, de Vries J, Ishakoglu K, Beld E, Lagendijk J, Raaymakers B (2016) Minimizing the magnetic field effect in MR-linac specific QA-tests: the use of electron dense materials. Phys Med Biol 61(3):N50–N59
24. Budgell G, Brown K, Cashmore J, Duane S, Frame J, Hardy M, Paynter D, Thomas R (2016) IPEM topical report 1: guidance on implementing flattening filter free (FFF) radiotherapy. Phys Med Biol 61:8360–8394
25. Palmer A, Dimitriadis A, Nisbet A, Clark C (2015) Evaluation of Gafchromic EBT-XD film, with comparison to EBT3 film, and application in high dose radiotherapy verification. Phys Med Biol 60:8741–8752
26. Lewis D, Micke A, Yu X (2012) An efficient protocol for radiochromic film dosimetry combining calibration and measurement in a single scan. Med Phys 39:6339–6349
27. Lewis D, Chan M (2015) Correcting lateral response artifacts from flatbed scanners for radiochromic film dosimetry. Med Phys 42:416–429

28. Hackett S, van Asselen B, Wolthaus J, Bluemink J, Ishakoglu K, Kok J, Lagendijk J, Raaymakers B (2018) Spiraling contaminant electrons increase doses to surfaces outside the photon beam of an MRI-linac with a perpendicular magnetic field. Phys Med Biol 63:095001. https://doi.org/10.1088/1361-6560/aaba8f
29. Baines J, Powers M, Newman G (2021) Sources of out-of-field dose in MRgRT: an inter-comparison of measured and Monaco treatment planning system doses for the Elekta Unity MR-linac. Phys. Eng. Sci. Med. *Accepted for publication.*
30. O'Brien D, Dolan J, Pencea S, Schupp N, Swawkuchi G (2017) Relative dosimetry with an MR-linac: Response of ion chambers, diamond, and diode detectors for off-axis, depth dose, and output factor measurements. Med Phys 45(2):884–897
31. Pojtinger S, Nachbar M, Kapsch RP, Thorwarth D (2020) Influence of beam quality on reference dosimetry correction factors in magnetic resonance guided radiation therapy. Physics Imaging in Radiation Oncology 16:95–98. https://doi.org/10.1016/j.phro.2020.10.005
32. Miften M, Olch A, Mihailidis D et al (2018) Tolerance limits and methodologies for IMRT measurement-based verification QA: Recommendations of AAPM Task Group No. 218. Med Phys 45:e53–e83

Tables

Tables 6-9 are not available with this version

Figures

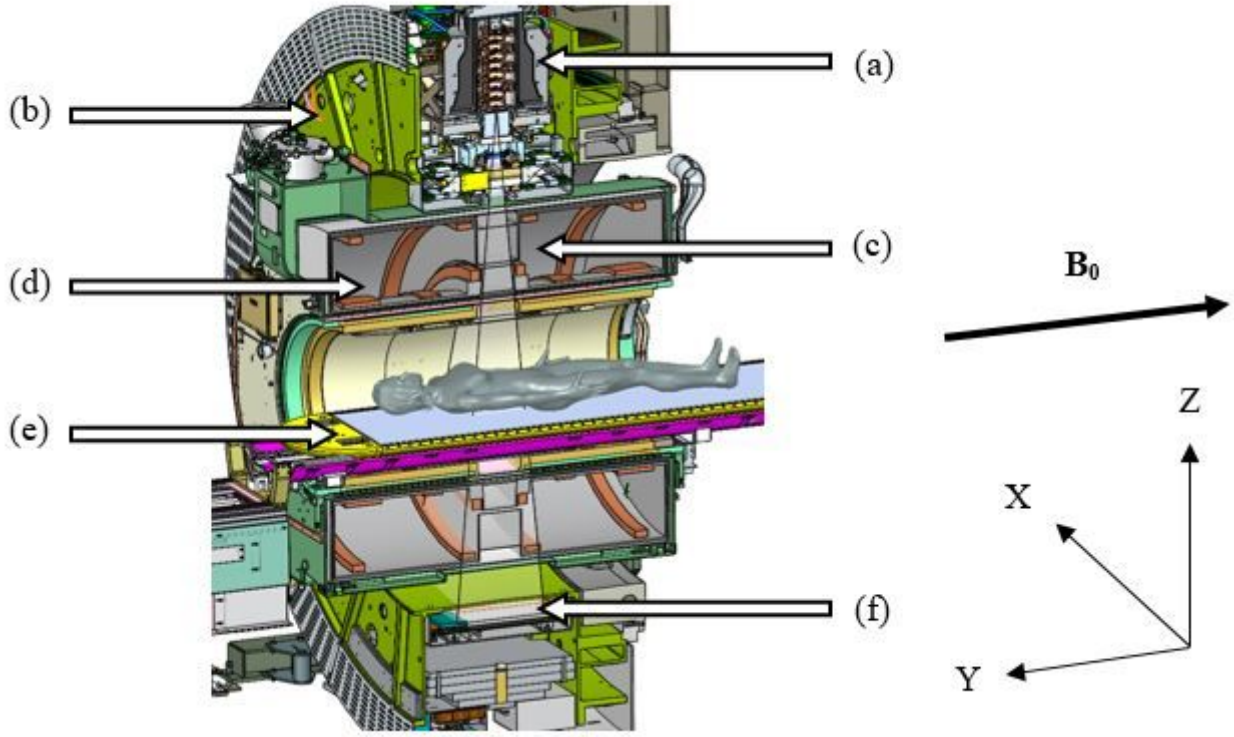

Figure 1

A schematic of the Elekta Unity MR-Linac, courtesy of Elekta, showing (a) the straight-through waveguide, (b) the gantry ring, (c) the primary radiation beam passing through (d) the coil system embedded in the magnet cryostat, (e) the patient positioning system and (f) the MVI for imaging. The IEC61217 coordinate system is shown, and for the head-first-supine patient orientation B0 is in the craniocaudal direction (negative Y)

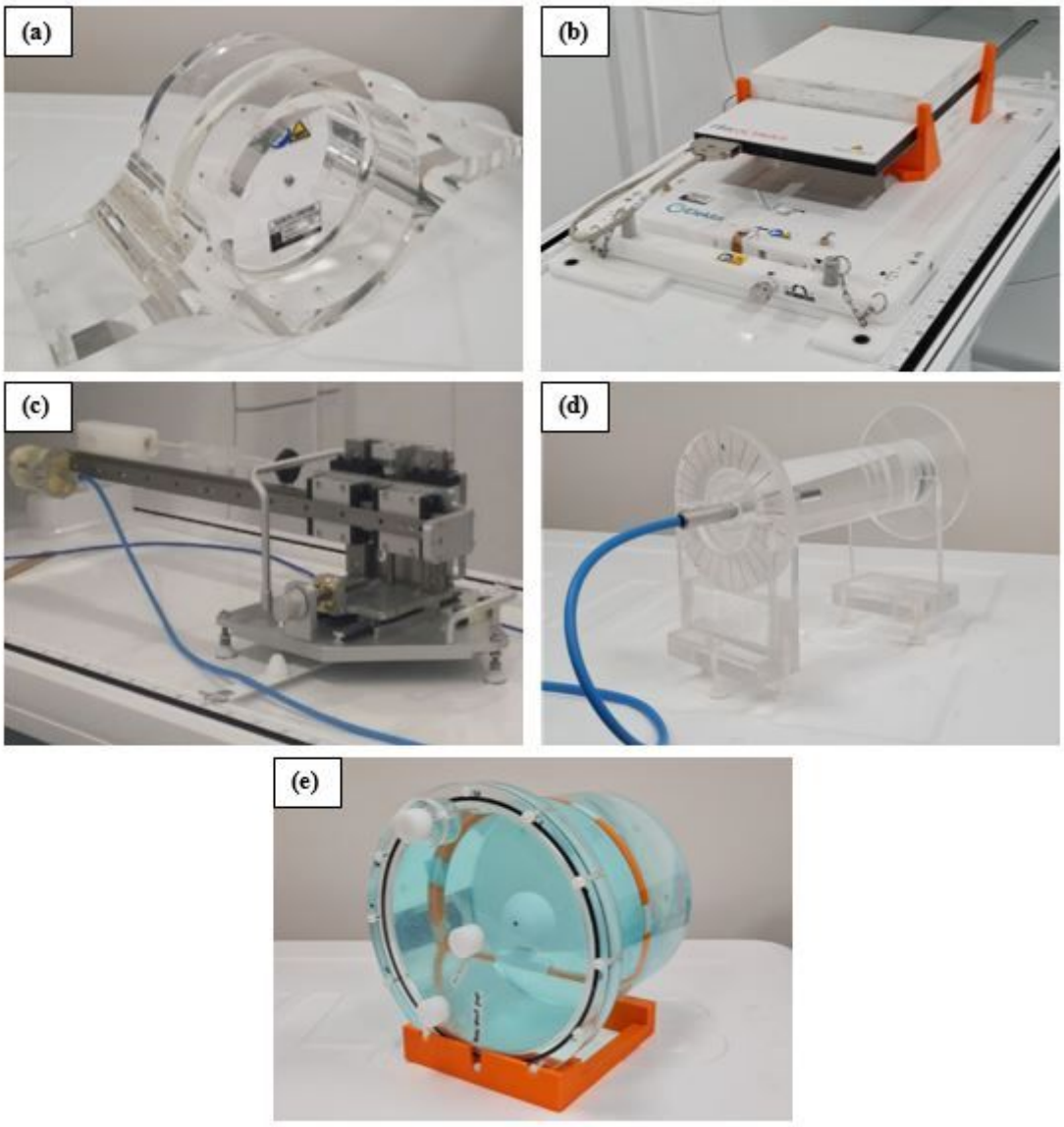

Figure 2

Images of the Elekta supplied (a) MV alignment phantom (b) QA Platform with the PTW Octavius 1500MR array and solid water stack (c) cryostat characterisation tool, as well as the in-house developed (d) cylindrical phantom used for rotational output measurements and (e) Perspex phantom shell used for E2E workflows

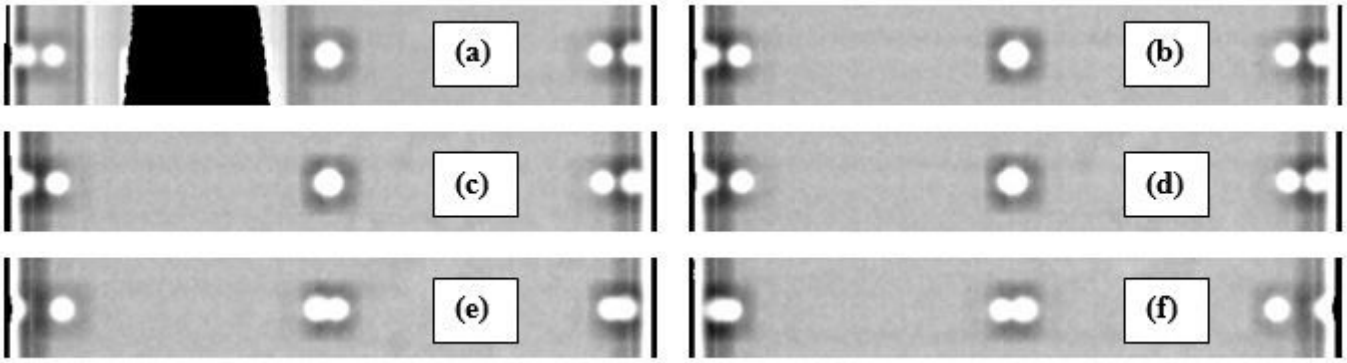

Figure 3

EPID images of the superior outer ring of ballbearings on the MV alignment phantom. Gantry angles of (a) 270°, (b) 0.0°, (c) 0.2°, (d) 0.3°, (e) 1.0° and (f) 359.0° are presented

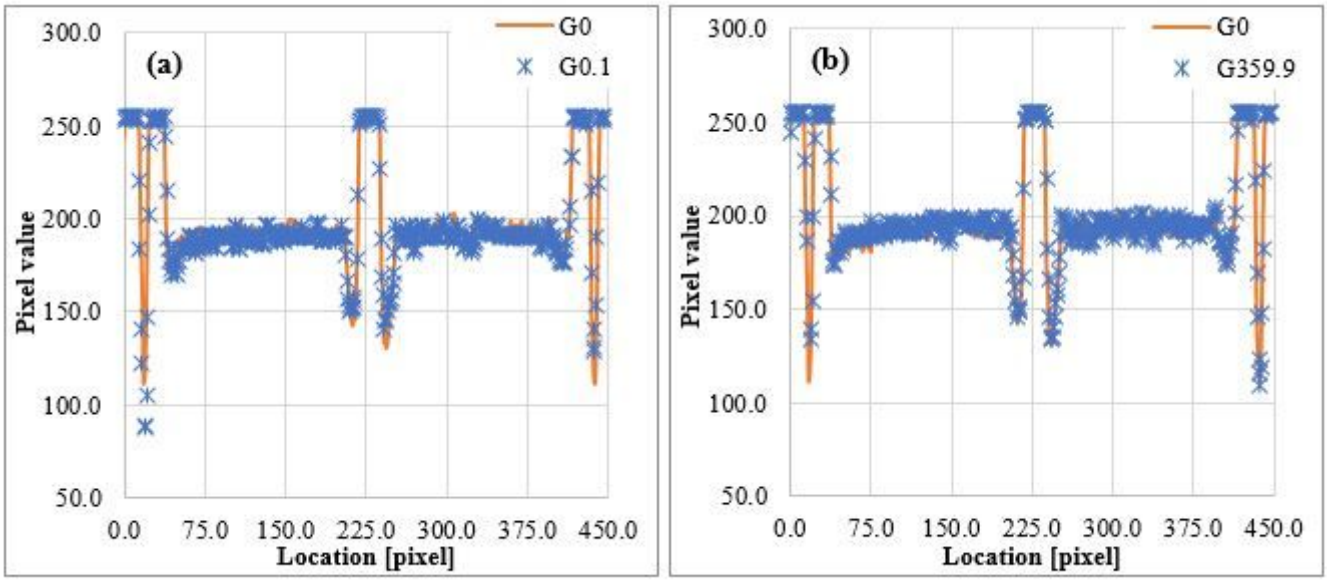

Figure 4

Comparison of profiles taken left to right from EPID images for the ballbearings at (a) G0 and G0.1 and (b) G0 and G359.9

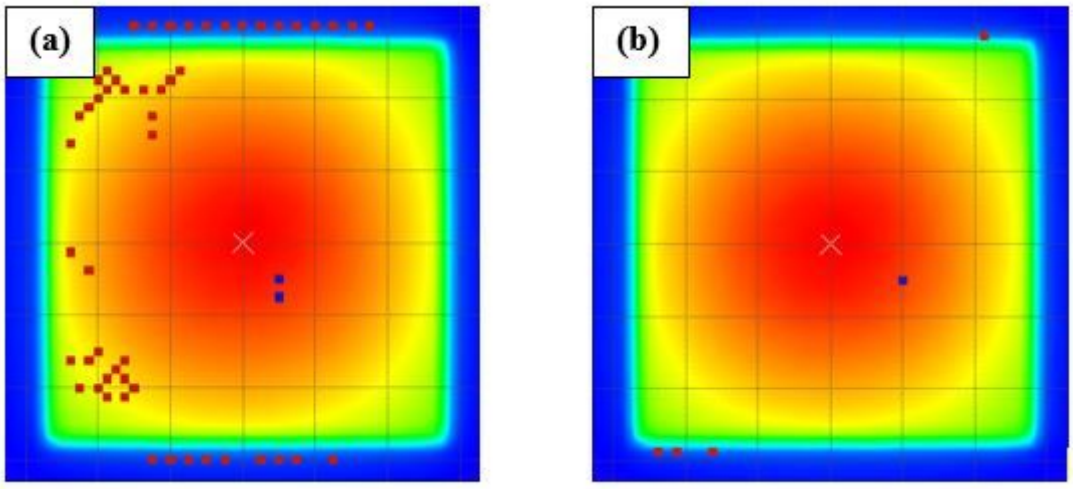

Figure 5

Dose maps for 22.0 × 22.0 cm2 fields measured on the Octavius 1500MR array and compared to TPS calculations using gamma analysis for (a) the original commissioning magnetron and (b) obtained with the new magnetron. Regions of hot/cold failure are indicated by the red/blue dots respectively

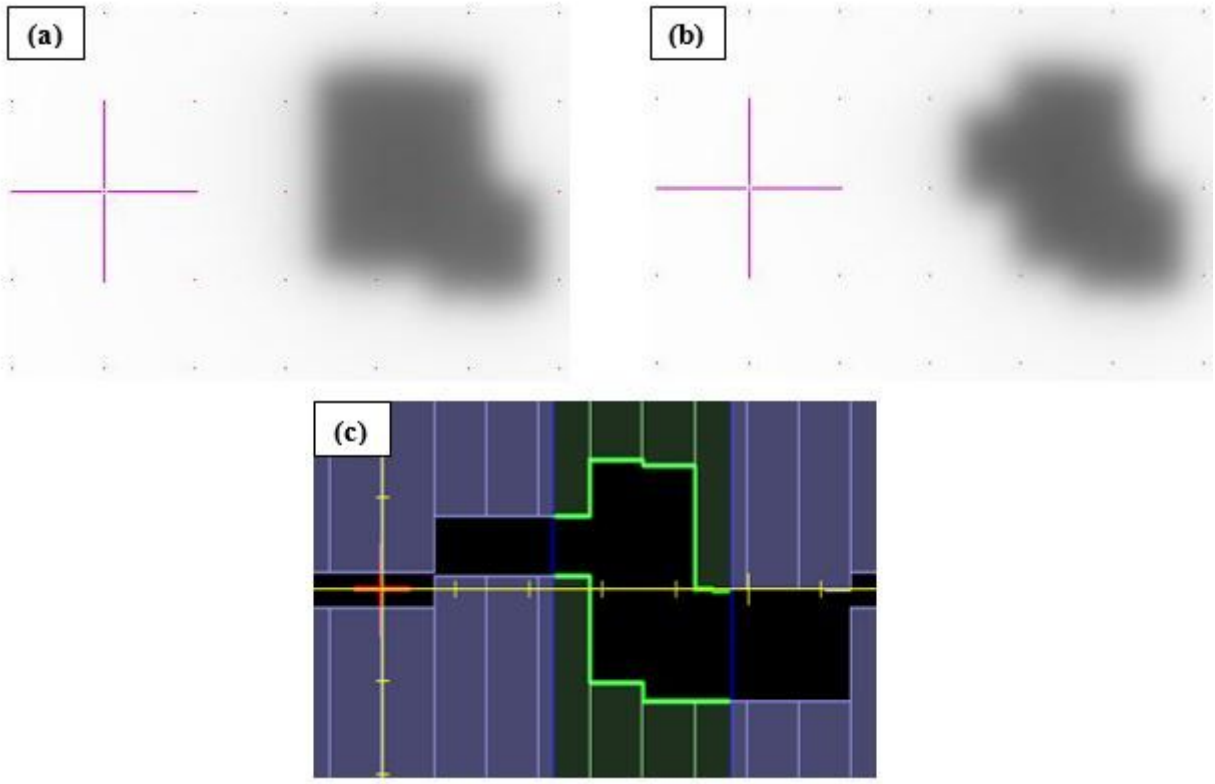

Figure 6

EPID images of two segments for one of the in-house developed stereo plans. (a) shows one delivered segment with the guard leaf error present and (b) shows the same segment with the error removed, matching that which was planned as indicated by (c) the beams-eye-view from Monaco TPS